

## Fretting Wear Behavior of Nano-Intermetallic Precipitates $Al_{65}Cu_{20}Ti_{15}$ Amorphous Matrix Composite Prepared by Pulse Plasma Sintering of the Ball Milled Powder

D. Roy<sup>1\*</sup>, O.A.Ojo<sup>2</sup>, H. Raghuvanshi<sup>3</sup> and A. Basu<sup>4</sup>

<sup>1</sup>Materials and Metallurgical Engineering Department, NIFFT, Ranchi-834003, India

<sup>2</sup>Mechanical and Manufacture Engineering Department, University of Manitoba, Winnipeg, Canada- R3T2N2

<sup>3</sup>Manufacturing Engineering Department, NIFFT, Ranchi-834003, India

<sup>4</sup>Metallurgical and Materials Engineering Department, NIT Rourkela, Rourkela-769008, India

### Abstract

In selection and design of materials for tribological applications, high resistance to material damage or least surface deterioration of the contacting surfaces is of considerable interest. The present work deals with the study of the wear properties investigated under fretting condition of  $Al_{65}Cu_{20}Ti_{15}$  composite containing finely distributed intermetallic compounds, fabricated by mechanical alloying followed by pulse plasma sintering (PPS) process. The wear experiments were carried out in gross slip fretting conditions to investigate the wear performance of the composite against the  $Al_2O_3$  balls with ambient conditions of temperature ( $24 \pm 2^\circ C$ ) and humidity ( $50 \pm 5\%$ ).

**Keywords:** Fretting; Metal matrix composite; Electron microscopy; Profilometry

### Introduction

Al alloys have found a wide variety of uses in transportation engineering application due to their high strength-to-weight ratios. However, conventional Al alloys exhibit a poor wear resistance and their applications have often been restricted when wear resistance is required. In recent years Al based metal matrix composites (MMCs) have been receiving considerable attention for their better wear resistance. Two approaches have been reported: (a) incorporation of hard phases into Al alloys, such as ceramic particles [1,2], (b) incorporation of soft solid-lubricants into Al alloys, such as graphite, mica and MoS<sub>2</sub> [3-5] by casting or by powder metallurgical routes. The tribological performance of these composite have been a subject of interest, especially for the potential applications in automobile components including cylinder block, piston and brake discs [6]. The wear tests are usually conducted under sliding wear condition by using pin-on-disc or block-on-ring tests. Though high volume fraction of hard reinforcements are favoured for wear resistance, the wear rate of the counterbody is found to be greatly enhanced by the abrasive action of the reinforcements [7,8]. Moreover, the high temperature strength is not improved because the reinforcement is too coarse to contribute to dispersion strengthening [9]. There is thus need for the development of new Al alloys which have good wear resistance and high strength.

Mechanical alloying is a solid state process which consists of the repeated welding, fracturing and rewelding of powder particle in highly energetic ball mill [10]. Several Al-based amorphous and nano-intermetallic dispersed amorphous matrix Al-alloys have been synthesized by mechanical alloying or melt-spinning in the recent past [11,12]. However the amorphous alloys in the form of ribbon, film and powder are not suitable for structural applications, unless bulk components are produced from such ribbons or powders. Hot pressing or hot extrusion is a possible route for consolidating powders into bulk sample or component [13,14]. It is known that mechanical properties of nanocrystalline materials are highly sensitive to the presence of internal defects, heterogeneities and grain size distributions [15,16]. In the recent years, Pulse Plasma Sintering (PPS) has emerged as a new sintering technique to obtain dense and near-net shaped bulk products from nanometer-size metallic powders. During such sintering an electric field is applied

(~ 600 MW) to activate and heat the powder by high current discharge pulses. The process has very high thermal efficiency and is similar to other plasma assisted sintering processed like spark plasma sintering and field assisted sintering (SPS) but differs in terms of the quantum of energy delivered and crucible design [17,18]. In this process, the powder compact is subjected to cycles of very rapid heating and cooling with very short holding time at the sintering temperature, lower than that of normal hot pressing [19]. The literature concerning the wear behaviour of mechanically alloyed Al alloys is very limited at present. The performance of materials in unlubricated contacts subjected to low amplitude oscillatory sliding, known as fretting wear, is of great importance. Fretting wear often occurs in mechanical joints of vibrating structures ranging from household appliances, automobiles, and aircraft to electrical equipment and even in human implants [20]. In the present work, fretting wear of a new generation nano-intermetallic reinforced Al based amorphous/nanocrystalline matrix composite is investigated. An effort has also been made to understand the operative wear mechanism.

### Experimental Procedure

#### Processing and characterization of composite

Appropriate amounts of Al-Cu-Ti elemental powders (with each constituent having at least 99.5 wt% purity and about 50–100  $\mu m$  particle size) in the nominal stoichiometry of  $Al_{65}Cu_{20}Ti_{15}$  were subjected to mechanical alloying in a Retsch PM 400 high-energy planetary ball mill, operated at 300 rpm with 10:1 ball to powder weight ratio us-

**\*Corresponding author:** D. Roy, Materials and Metallurgical Engineering Department, NIFFT, India. Tel: +91 651 229 1125; Fax: +91 651 2290860, E-mail: [Droy2k3@yahoo.co.in](mailto:Droy2k3@yahoo.co.in)

Received March 22, 2012; Accepted April 11, 2012; Published April 16, 2012

**Citation:** Roy D, Ojo OA, Raghuvanshi H, Basu A (2012) Fretting Wear Behavior of Nano-Intermetallic Precipitates  $Al_{65}Cu_{20}Ti_{15}$  Amorphous Matrix Composite Prepared by Pulse Plasma Sintering of the Ball Milled Powder. J Material Sci Eng 1:107. doi:10.4172/2169-0022.1000107

**Copyright:** © 2012 Roy D, et al. This is an open-access article distributed under the terms of the Creative Commons Attribution License, which permits unrestricted use, distribution, and reproduction in any medium, provided the original author and source are credited.

ing tungsten carbide (WC) coated vial and balls (10mm diameter). Mechanical alloying was carried out for 25 h, until a fully amorphous  $\text{Al}_{65}\text{Cu}_{20}\text{Ti}_{15}$  alloy was obtained. Thereafter, batches containing 2.5-3 g of amorphous  $\text{Al}_{65}\text{Cu}_{20}\text{Ti}_{15}$  alloy powder were loaded in cylindrical graphite die placed in a chamber evacuated up to the pressure of  $5 \times 10^{-2}$  Pa and subjected to a uniaxial load of 50 MPa for pulse plasma sintering. During sintering, the temperature on the surface of the graphite die was measured using an Ahlborn IR AMIR 7838-51 temperature transducer. The die was designed to yield sintered specimens of 15 mm diameter and 5 mm height. The temperature and heating rate of the sample were controlled by regulating the pulse discharge energy and pulse repetition frequency. The sintering process involved had two distinct stages that differed in terms of parameters, heating conditions and processing time. In the first stage, the powder charge was heated to a temperature of 200°C for 180 s. In the second stage, the discharge energy was increased and the sample was heated to the sintering temperatures of 400, 500 and 600°C.

Identity of the phases following high pressure sintering was determined by X-ray diffraction (XRD) using a Panalytical X'Pert Pro diffractometer with Cu K $\alpha$  (0.1542 nm) radiation. Electron transparent thin foils were prepared for Transmission Electron Microscope (TEM) studies using mechanical polishing followed by argon ion thinning using a GATAN precision ion mill for 30min. Selected foils prepared from composites sintered at 500 and 600°C were examined under a JEOL JEM 2100 High Resolution Transmission Electron Microscope (HRTEM) operated at 200 kV, using both bright and dark field as well as high resolution lattice imaging conditions. Selected Area Diffraction (SAD) was used to identify the phases present. Qualitative information on chemical compositions at different locations was obtained using the Energy Dispersive X-ray (EDX) analyzer (Oxford, UK) equipped with an ultra-thin window and attached to the HRTEM.

### Fretting wear tests

The fretting experiments were carried out using a computer controlled fretting machine (DUCOM, India). This machine produces a linear relative oscillatory motion with ball-on-flat configuration at a constant normal load. It was also equipped with an inductive displacement transducer, used to monitor the displacement of the samples. To record the friction force, it has a piezoelectric transducer. The samples were subjected to oscillations under 10N load against the  $\text{Al}_2\text{O}_3$  balls having diameter of 6 mm at a frequency of 8 Hz for a duration of 10,000 cycles with ambient conditions of temperature ( $24 \pm 2^\circ\text{C}$ ) and humidity ( $50 \pm 5\%$ ). The coefficient of friction was calculated from the measured friction force. The wear scar geometry (width, depth and contour) was traced at specific locations and orientation using a contact type stylus profilometer (Model Dektak 150 Veeco Instruments, USA) at a load of 3 mg force and diameter (both in the sliding and in the transverse direction). These dimensions were verified from relevant micrographs.

The worn surfaces generated due to wear testing were examined under a Field Emission Scanning Electron Microscope (FESEM, Zeiss, Supra-40).

### Results and Discussion

Figure 1 shows the XRD patterns of  $\text{Al}_{65}\text{Cu}_{20}\text{Ti}_{15}$  elemental powder blend, subjected to mechanical alloying in a planetary ball mill for 1 and 25 h, respectively. The inset shows the SAD pattern of the milled product after 25 h of mechanical alloying. It is evident that the XRD peaks representing the constituent elements disappear giving way to a broad halo after 25 h of ball milling. Absence of the characteristic

peaks, and presence of a broad halo corresponding to  $2\theta$  values between  $33^\circ$  and  $50^\circ$  with a corresponding diffused intensity halo in the SAD pattern confirms that the milled product after 25 h is predominantly amorphous, which is in agreement with the results of a previous study dealing with the same composition [21].

Figure 2 shows the results of XRD analysis of the mechanical alloyed powders consolidated by pulse plasma sintering. The patterns suggest that sintering has led to partial crystallization of the as-milled amorphous aggregate and yields a metastable composite microstructure comprising of several ultrafine intermetallic phases like  $\text{Al}_3\text{CuTi}_2$ ,  $\text{Al}_4\text{Cu}_3$ ,  $\text{Al}_2\text{Cu}$  and  $\text{Al}_3\text{Ti}$  in varying volume fractions dispersed in the amorphous matrix.

A bright field TEM image and the corresponding SAD pattern from the composite processed by PPS at 500°C are shown in Figure 3. Examination of the TEM image (Figure 3a) and indexing of the Debye rings in the corresponding SAD pattern (Figure 3b) indicate that nano-sized ( $\sim 50$  nm) precipitates of  $\text{Al}_3\text{Ti}$ ,  $\text{Al}_4\text{Cu}_3$  and  $\text{Al}_3\text{CuTi}$  are dispersed in the Al-rich partially amorphous matrix of the composite consolidated at 500°C. Figure 4 shows the bright field TEM image and the corresponding SAD pattern of the composite consolidated at 600°C. Comparison of the TEM images in Figure 3a and 4a suggests that

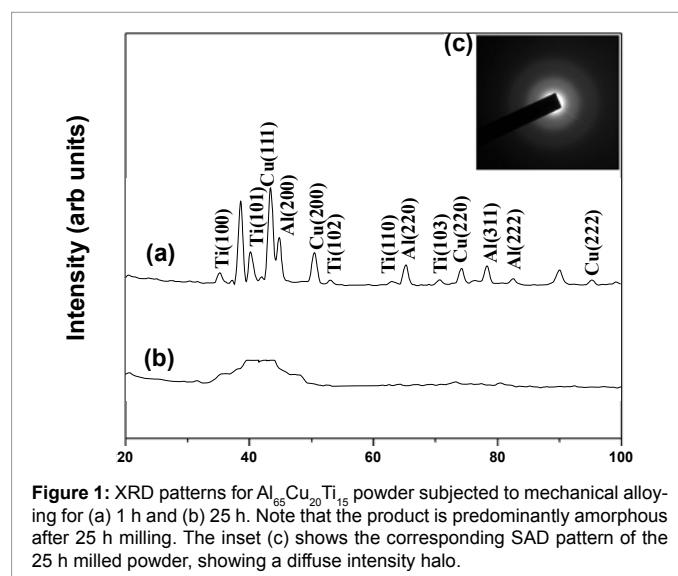


Figure 1: XRD patterns for  $\text{Al}_{65}\text{Cu}_{20}\text{Ti}_{15}$  powder subjected to mechanical alloying for (a) 1 h and (b) 25 h. Note that the product is predominantly amorphous after 25 h milling. The inset (c) shows the corresponding SAD pattern of the 25 h milled powder, showing a diffuse intensity halo.

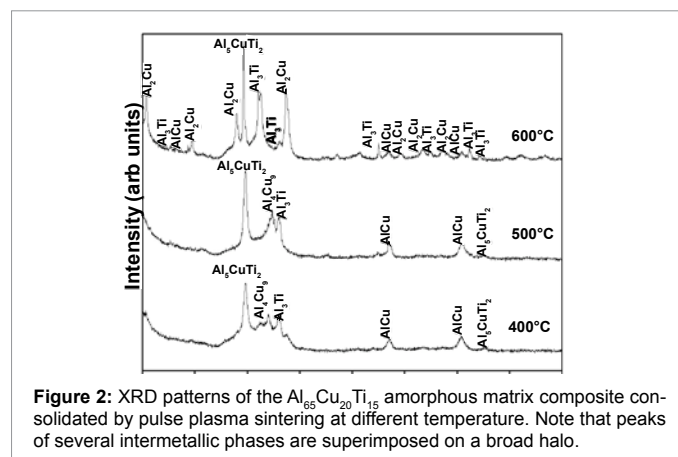


Figure 2: XRD patterns of the  $\text{Al}_{65}\text{Cu}_{20}\text{Ti}_{15}$  amorphous matrix composite consolidated by pulse plasma sintering at different temperature. Note that peaks of several intermetallic phases are superimposed on a broad halo.

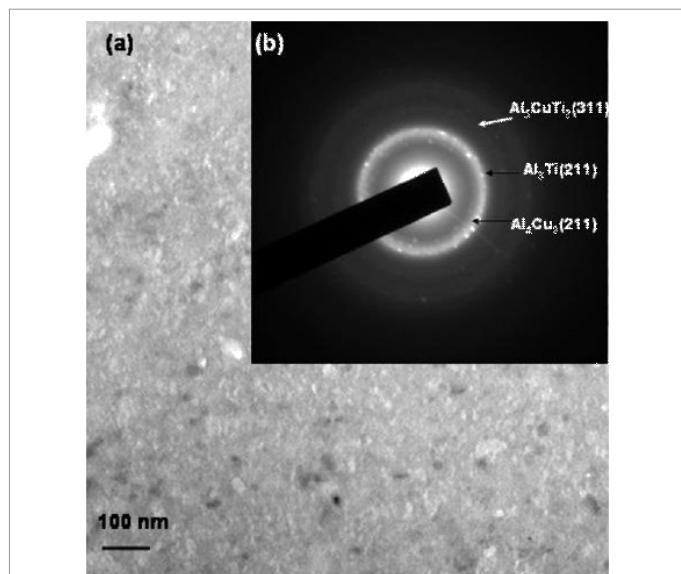


Figure 3: (a) Bright field TEM image and inset (b) the corresponding SAD pattern of the composite prepared by PPS at 500°C.

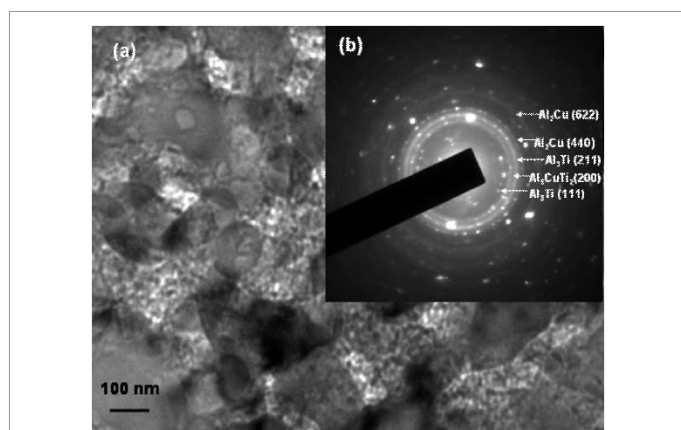


Figure 4: (a) Bright field TEM image and inset (b) the corresponding SAD pattern of the composite prepared by PPS at 600°C.

Sample identification	Processing Temperature (°C)	Density Mg/m <sup>3</sup>	Nano-hardness(GPa)	Young's Modulus(GPa)	Indentation Fracture toughness(MPa√m)	Compressive Stress (MPa)
	400	3.17	2.1	44	2.34	430
$Al_{65}Cu_{20}Ti_{15}$	500	3.67	9.0	140	4.63	1760
	600	3.73	14.0	208	4.23	1588

Table 1: Summary of mechanical properties of the  $Al_{65}Cu_{20}Ti_{15}$  amorphous/nanocrystalline composite processed at different temperatures.

the volume fraction of the crystalline phase is greater in the sample sintered at higher (600°C) temperature. In fact, the SAD pattern from the composite sintered at 600°C (Figure 4b) shows prominent and sharp Debye rings, practically without the diffuse halo contributed by the amorphous region. In other words, the rings of the SAD pattern in Figure 4b represent a predominantly nanocrystalline structure.

Table 1 presents the summary of the mechanical properties of the  $Al_{65}Cu_{20}Ti_{15}$  amorphous/nanocrystalline composite processed at different temperatures. The details of the processing, microstructure and

mechanical properties of the investigated composites can be found elsewhere [22].

### Fretting wear

The effect of the sintering temperature of the amorphous matrix composites on the frictional behavior during fretting against the  $Al_2O_3$  ball is as shown in the plots of Coefficient of Friction (COF) versus the number of cycles in Figure 5. Analyzing the plots clearly tells us that the steady-state COF of the composite sample sintered at 500°C is lower than the samples sintered at 400°C and 600°C. For the composite samples sintered at 400°C and 600°C, the COF rises rapidly from a very low value during the running in period (first 1500 cycles) to reach a steady-state value. However in the composite sample sintered at 500°C, the COF does not show an abrupt rise and increases gradually to a value which is lower than the other two composite samples.

After the fretting wear tests, the wear scar diameter (transverse to the fretting direction) and the displacement amplitude have been measured and the volume of the worn surface has been calculated according to the formulation proposed by Klaffke [23].

where V is the wear volume, R the radius of ball (6 mm), d the diameter of wear scar in the transverse direction, and A the displacement amplitude (80 μm).

Figure 6 shows a typical front view of the worn/damaged region

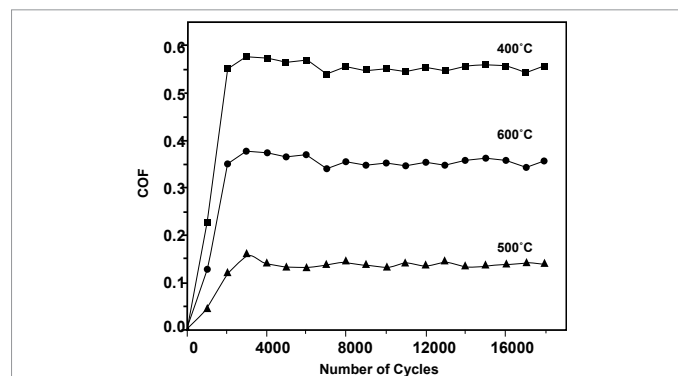


Figure 5: Variation of Coefficient of Friction (COF) versus Number of Cycles of fretting wears showing the different sintering temperatures.

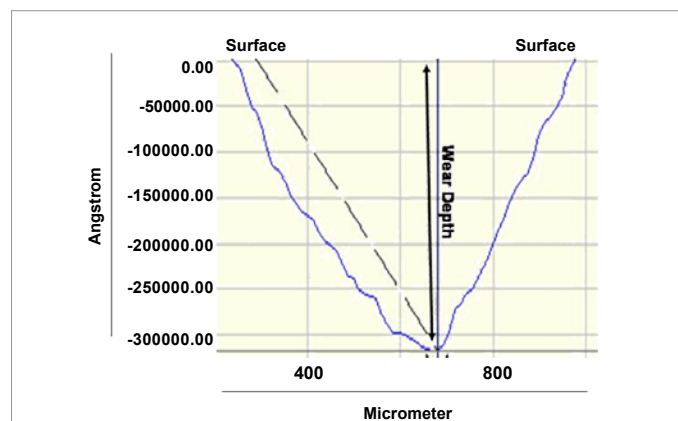


Figure 6: Surface contour of worn surface across the fretting wear track on the vertical (cross-sectional) plane perpendicular to the top surface and wear direction. The contour was determined at the middle of the wear track using a surface profilometer.

caused by fretting wear (as viewed on the cross-sectional plane perpendicular to both fretting direction and wear/top surface). From the surface profilometer data shown in Figure 6 it is apparent that the depth of worn surfaces of the alloys sintered at 500°C is greater at the centre than that at the periphery.

Bar charts depicting the wear volumes as measured in the fretting tests carried out on the nano-intermetallic reinforced Al<sub>65</sub>Cu<sub>20</sub>Ti<sub>15</sub> composite sintered at three different temperatures is shown in Figure 7. The error bars in the wear results indicate the scatter in the data (standard deviation) obtained from the results of at least three identical tests. It is evident from Figure 7 that the wear volume is the least and hence the wear resistance is the highest for the sample sintered at 500°C. Thus, sintering at 500°C appears to produce the strongest and wear resistant component in the present study. Lower steady COF and lower wear loss is better for tribological applications and in the present study both of them show similar trend, i.e. sample sintered at 500°C shows best result, sample sintered at 400°C shows worst result and 600°C sample is the intermediate one. From Figure 2 it is evident that phase evolution/crystallization are similar in 400 and 500°C sintered sample and it is also reported that hardness/strength is better in 500°C due to better sintering/bonding. Due to the same reason sample sintered at 500°C shows better tribological property than 400°C sample. But the same trend is not continued in 600°C sample due to formation of more types of brittle intermetallics (Figure 2). Hard worn out particle acts as third body resulting in higher COF and wear loss compared to 500°C sample. It is also worth mentioning that though 600°C sintered sample show higher hardness, wear trend is different as fretting wear is not a static loading test as compared to hardness test in the scenario when phase formation/crystallization amount is different. The morphological features on the worn surfaces have been investigated using FESEM in an attempt to study the wear mechanism. Figure 8a and b reveals

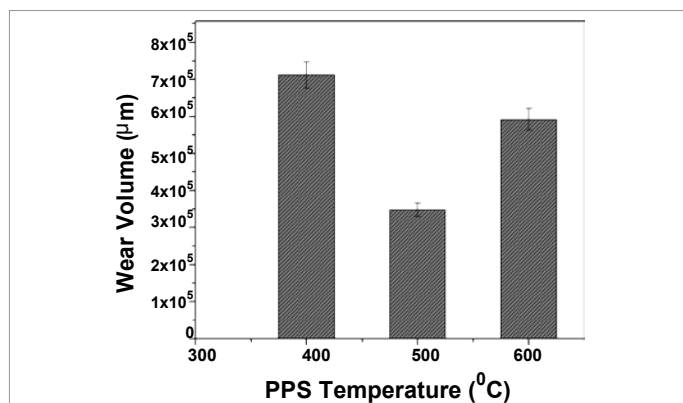


Figure 7: Bar chart depicting the values of wear volume of the composite samples sintered at 400, 500 and 600°C.

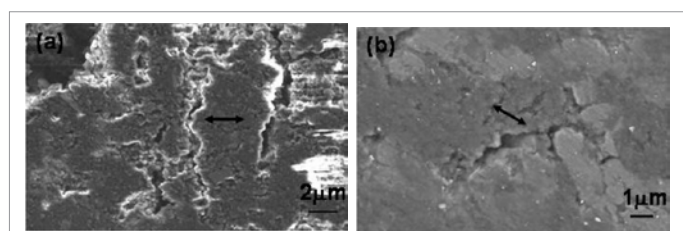


Figure 8: (a,b) FESEM images depicting the morphological features of the worn surfaces of the nano-intermetallic reinforced Al<sub>65</sub>Cu<sub>20</sub>Ti<sub>15</sub> amorphous matrix composite sintered at 500°C.

the extent of wear damage on the worn surface of mechanically alloyed Al<sub>65</sub>Cu<sub>20</sub>Ti<sub>15</sub> sample compacted and sintered at 500°C at low and high magnification, respectively. This difference in the extent of damage appears to be a strong evidence of localized plastic deformation during fretting wear. Examination of the FESEM image in Figure 8b indicates that micro-cracks are present on the worn surface of the alloy sintered at 500°C.

To understand the wear mechanism better, we further study the changes in the chemical composition of the worn surface during fretting wear. Figure 9 (a) shows the microstructure as well as the EDS X-ray line scans of Al, Cu, Ti and O obtained by the EDS analysis of the worn and unworn locations on the composite samples sintered at

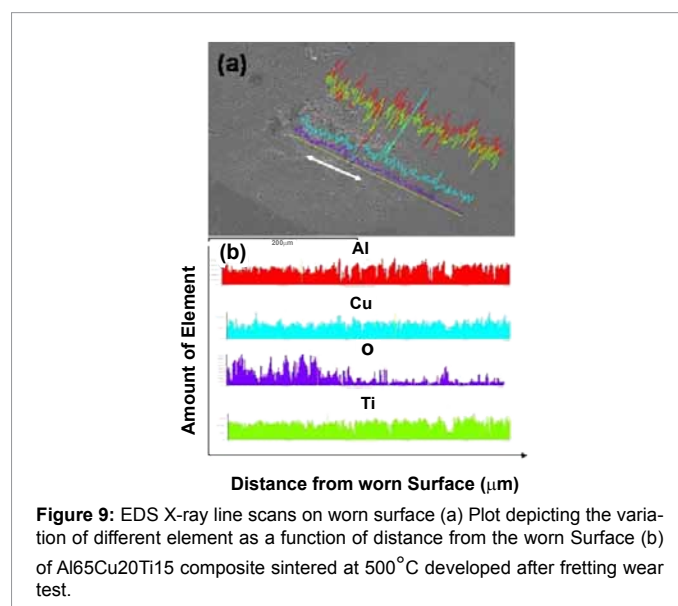


Figure 9: EDS X-ray line scans on worn surface (a) Plot depicting the variation of different element as a function of distance from the worn Surface (b) of Al<sub>65</sub>Cu<sub>20</sub>Ti<sub>15</sub> composite sintered at 500°C developed after fretting wear test.

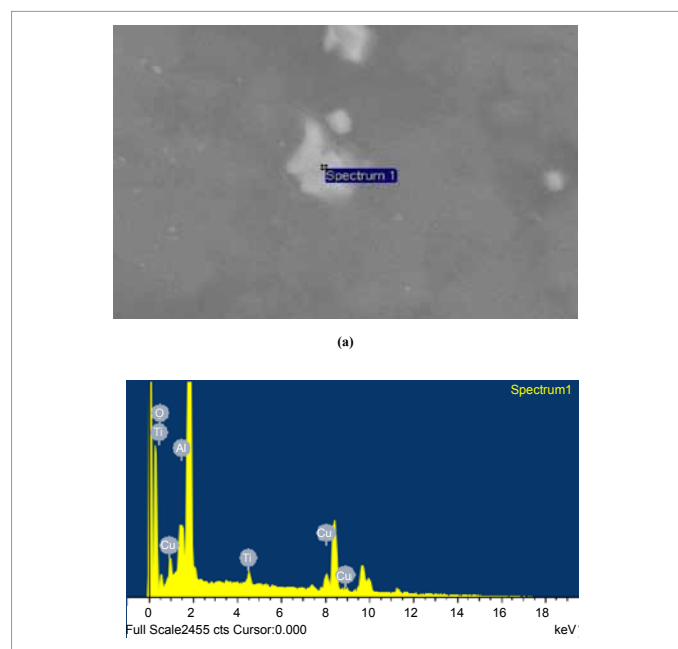


Figure 10: Field emission scanning electron micrograph (a) EDS Spectrum of the wear debris (b) on Al<sub>65</sub>Cu<sub>20</sub>Ti<sub>15</sub> composite Pulse plasma sintered at 600 °C developed after fretting wear test.

500°C. The X-ray line scans of the surface are shown at higher magnification in Figure 9 (b). On comparison of the peak heights of the X-ray line scans, qualitatively representing the relative oxygen content at the worn and unworn locations on the surface, it is obvious from the scans that the intensity of the peaks is higher in case of the worn locations. In other words the worn locations are more enriched in Oxygen than the unworn location which confirms that the wear is also oxidative in nature. In this type of mechanism, the frictional heating during fretting cause oxidation of the surface, which in turn accelerates wear through the removal of the oxide fragments. The greater damage encountered during fretting wear of the composite sintered at 600°C than on the composite sintered at 500°C can be attributed to the fact that the intermetallic particulates at or near the worn surfaces are more prone to oxidation than the amorphous phase and contribute to the formation of coarser wear debris. This is better understood through the EDS spectrum of the wear debris as shown in Figure 10. The XRD results indicate the formation of a number of complex crystalline intermetallics like Al<sub>3</sub>Ti and Al<sub>5</sub>CuTi<sub>2</sub> in the composite sintered at 600°C. Since the grain boundaries of the crystalline intermetallic phases are expected to provide the short circuit paths for the diffusion of Oxygen anions, it is quite clear that the composite sintered at 500°C with a higher volume fraction of the amorphous phase is more resistant to fretting wear and hence the wear volume is lesser than the composite sintered at 600°C confirming earlier claim of more wear resistant property in 500°C sintered sample.

## Conclusions

Under the investigated tribological condition with Al<sub>2</sub>O<sub>3</sub> as counter-body, the present Al-based amorphous + nanocrystalline composites experience frictional behavior with steady state coefficient of friction ranging between 0.15 and 0.55. The wear behavior of the Al<sub>65</sub>Cu<sub>20</sub>Ti<sub>15</sub> nanocrystalline + amorphous composite critically depends on the sintering temperature and phase aggregate in the microstructure. The Al<sub>65</sub>Cu<sub>20</sub>Ti<sub>15</sub> composite exhibits the highest wear resistance when sintered at 500°C which is due to the higher fraction of the amorphous phase as compared to the one sintered at 600°C.

## Acknowledgement

The authors express their sincere gratitude to Professor Indranil Manna, Director, CGCRI, Kolkata and Professor Rahul Mitra, Indian Institute of Technology, Kharagpur, India for their valuable suggestion and discussion in connection to this research work. Thanks are also due to Professor Michalski (Warsaw University of Technology, Poland) for access to Pulse Plasma Sintering.

## Reference

1. Alpas AT, Zhang J (1992) Effect of SiC particulate on dry sliding wear of Al-Si alloys (A356) *Wear* 155: 83-104.
2. Lee CS, Kim YH, Han KS, Lim T, (1992) Wear behaviour of Al matrix composite materials. *J Mater Sci* 27: 793-800.
3. Zamzam MA (1989) Wear resistance of agglomerated and dispersed solid lubricants. *Al Mater Trans JIM* 30: 516-522
4. Liu Y, Rohatgi PK, Ray S (1993) Tribological Characteristics of Al-50vol pct graphite composite. *Metall Trans A* 24:151-159.
5. Nath D, Biswas SK, Rohatgi PK (1980) Wear characteristics and bearing performance of Al-Mica particulate composite material. *Wear* 60: 61-67.
6. Hutchings IM (1994) Wear-resistance materials: into the next century. *Mater Sci Eng A* 18:185-195.
7. Wood JV, Davies P, Kellie JLF (1993) Properties of reactively cast Al-TiB<sub>2</sub> alloys. *Mater Sci Technol* 9: 833-840.
8. Wang A, Back HJ (1991) Dry sliding wear in 2124 Al-SiCw/17-4PH stainless steel systems. *Wear* 147: 355-374.

9. Nieh TG, McNally CM, Wadsworth J, Yaney DL, Gilman PS, (1988) Mechanical properties of a SiC reinforced Al composite prepared by mechanical alloying, in Y.W.Kim and W.M.Griffith (eds), *Dispersion Strengthened Al Alloys*, TMS, Warrendale pp 681-691.
10. Gilman PS, Benjamin JS (1983) Mechanical alloying. *Annu Rev Mater Sci* 13: 279-300.
11. Li JC, Zhao ZK, Jiang Q (2003) Mechanical Properties of High-strength Al90Mn8Ce2 Alloy *Adv Eng Mater* 5: 119-122.
12. Li JC, Zhao ZK, Jiang Q, (2003) Properties of High Strength Al85La10Ni5 Alloy. *Mater Sci Eng A* 339: 205-208.
13. Y Kawamura, H Mano, A Inoue (2001) Nanocrystalline aluminum bulk alloys with a high strength of 1420 MPa produced by the consolidation of amorphous powders *Scripta Mater* 44: 1599-160.
14. F Schurack, J Eckert, L Schultz (2000) Quasicrystalline Al-alloys with high strength and good ductility *Mater Sci Eng A* 294: 164-167.
15. Kumar KS, Swygenhoven H, Suresh S (2003) Mechanical behaviour of nanocrystalline metals and alloys. *Acta Mater* 51: 5743-5774.
16. Sun XK, Cong HT, Sun M, Yang MC, (2000) Preparation and mechanical properties of highly densified nanocrystalline Al *Metall Mater Trans A* 31: 1017-1024.
17. M Rosinski, A Michalski (2006) Nanocrystalline NiAl-TiC Composites Sintered by the Pulse Plasma Method *Solid State Phenom* 114: 233-238.
18. A Michalski, M Rosinski, D Siemiaszko, J Jaroszewicz, J Kurzydowski (2006) Pulse Plasma Sintering of nanocrystalline Cu Powder. *Solid State Phenom* 14: 239-234.
19. Xu CY, Jia SS, Cao ZY (2005) Synthesis of Al-Mn-Ce alloy by the spark plasma sintering, *Mater Charact* 54: 394-398.
20. P Blanchard, C Colomble, V Pellerin, S Fayeulle, L Vincent (1991) Material effect in fretting wear: application to iron, titanium, and aluminium alloys. *Metall Trans A* 22: 1535-1544.
21. Nandi P, Chattopadhyay PP, Pabi SK, Manna I (2003) *Mater Sci Eng A* 359: 11-17.
22. D Roy, SS Singh, R Mitra, M Rosinski, A Michalski et al. (2009) Synthesis and characterization of precipitation hardened amorphous matrix composite by mechanical alloying and pulse plasma sintering of Al65Cu20Ti15 *Philosophical Magazine* 89: 1051-1061.
23. D Klaffke (1989) Fretting wear of ceramics. *Tribol Int* 22: 89-101.